Miscibility and Crystallization Kinetics of Poly(3-hydroxybutyrate-*co*-3-hydroxyvalerate)/ Poly(methyl methacrylate) Blends

Hsiu-Jung Chiu

Department of Chemical Engineering, Ta Hwa Institute of Technology, Chiunglin, Hsinchu, 30703, Taiwan, Republic of China

Received 20 December 2002; accepted 26 September 2003

ABSTRACT: The miscibility and crystallization kinetics of the blends of random poly(3-hydroxybutyrate-*co*-3-hydroxyvalerate) [P(HB-*co*-HV)] copolymer and poly(methyl methacrylate) (PMMA) were investigated by differential scanning calorimetry (DSC) and polarized optical microscopy (POM). It was found that P(HB-*co*-HV)/PMMA blends were miscible in the melt. Thus the single glass-transition temperature (T_g) of the blends within the whole composition range suggests that P(HB-*co*-HV) and PMMA were totally miscible for the miscible blends. The equilibrium melting point (T_m^o) of P(HB-*co*-HV) in the P(HB-*co*-HV)/PMMA blends decreased with increasing PMMA. The T_m^o depression supports the miscibility of the blends. With respect to the results of crystallization kinetics, it was found that both the spherulitic growth rate and the overall crystallization rate decreased with the addition of PMMA. The kinetics retardation was attributed to the decrease in P(HB-*co*-HV) molecular mobility and dilution of P(HB-*co*-HV) concentration resulting from the addition of PMMA, which has a higher T_g. According to secondary nucleation theory, the kinetics of spherulitic crystallization of P(HB-*co*-HV) in the blends was analyzed in the studied temperature range. The crystallizations of P(HB-*co*-HV) in P(HB-*co*-HV)/PMMA blends were assigned to $n = 4$, regime III growth process. © 2004 Wiley Periodicals, Inc. J Appl Polym Sci 91: 3595–3603, 2004

Key words: crystallization; poly(3-hydroxybutyrate-*co*-3-hydroxyvalerate); melting point; spherulites; miscibility

INTRODUCTION

Crystallization kinetics of melt-miscible blends of crystalline and amorphous polymers has been extensively studied.[1–15] When crystallization occurs below the melting point of the crystalline component, the process involves two types of polymer transport: diffusion of the crystallizable component toward the crystal growth front and a simultaneous rejection of the amorphous component. This crystallization process produces a liquid–solid phase separation, leading to a variety of morphological patterns closely governed by the kinetics of the two types of polymer transport. In this case, the morphological formation may be kinetically controlled by the thermal history and composition to achieve tailor-made properties for the blends. Therefore, investigation of the crystallization kinetics of polymer blends containing crystallizable components also has practical significance.

Correspondence to: hjc@thit.edu.tw.

Contract grant sponsor: National Science Council, Republic of China; contract grant number: NSC 91-2216-E-233-001.

Journal of Applied Polymer Science, Vol. 91, 3595–3603 (2004)

Bacterially synthesized poly(3-hydroxybutyrate) (PHB) is a crystalline polymer with biodegradable and biocompatibility characteristics, which are attractive for application in the present environment.[16–18] PHB also has some disadvantages such as high brittleness, poor processability, and poor thermal stability, which can be promoted kinetically by the PHB crystallization process. Crystallization kinetics of PHB in melt-miscible blends such as PHB/poly(epichlorohydrin) (PECH),[1,2] PHB/poly(vinyl acetate) (PVAc),[3–5] PHB/atactic-PHB,[6,7] and PHB/poly(vinyl phenol) (PVPh)[8,9] blends has been extensively studied. However, Lotti et al.[19] and Sicilano et al.[20] reported that PHB/PMMA blends containing up to 20 wt % PHB were miscible in the melt but, at rich-PHB compositions, were involved in a 20/80 PHB/PMMA miscible phase, whereas the excess PHB segregated and formed a partially crystalline phase. If P(HB-*co*-HV) were used instead of PHB, we would find the blends of P(HB-*co*-HV)/PMMA are miscible in the melt over the whole blend composition range.

In this study, we present our results obtained on the phase behavior and crystallization kinetics for the blends of P(HB-*co*-HV) and PMMA. It will be shown that this system exhibits miscibility. Further, it will be demonstrated that the addition of PMMA to P(HB-*co*-

HV) will result in a decrease in both the spherulitic growth rate and the overall crystallization rate.

EXPERIMENTAL

Materials and samples preparation

P(HB-*co*-HV) ($M_n = 1.41 \times 10^5$ and $M_w = 2.13 \times 10^5$) copolymer containing 10 mol % HV content, and PMMA ($M_n = 4.6 \times 10^4$ and $M_w = 9.3 \times 10^4$) were purchased from Fluka Chemical Co. (Buchs, Switzerland) and Aldrich Chemical Co. (Milwaukee, WI), respectively. P(HB-*co*-HV) was blended with PMMA by solution casting. The blending components were dissolved in DMF at room temperature, yielding a 1 wt % solution. The solution was subsequently poured onto a petri dish and the blend film was obtained after evaporating most of the solvent on a hot plate at about 90°C. The blend film was further dried in a vacuum oven at 50°C for at least 24 h until a constant sample weight was achieved. TGA measurement of the dried films showed negligible weight loss above the boiling point of DMF, indicating nearly complete removal of solvent for the blend films.

Polarized optical microscopy

The spherulitic morphology and growth rate were monitored with a Zeiss polarized optical microscope (Zeiss, Oberkochen, Germany). The sample was first melted on a Linkam HFS91 hot stage at 190°C for 1 min, then quickly transferred to another hot stage equilibrated at the desired crystallization temperature (T_c), where spherulitic growth was monitored. Micrographs were taken at intervals for measuring the spherulitic radii (R) at various time periods. The growth rate was calculated from the change of spherulitic radius with time, dR/dt.

Differential scanning calorimetry

Differential scanning calorimetry was performed with a TA 2000 DSC (TA Instruments, New Castle, DE), which was calibrated with indium before use. The sample was heated to 190°C for 1 min, and then quickly quenched to −50°C with liquid nitrogen. Subsequently, the glass-transition temperature (T_g), cold crystallization temperature (T_{cc}), and melting-point temperature (T_m) were measured by reheating the sample from −50 to 190°C at a heating rate of 20°C/min. For the Hoffman–Weeks plots, the sample was heated to 190°C for 1 min and then quenched to the desired crystallization temperature (T_c) crystallized for 1 h. Subsequently, T_m was measured at a heating rate of 20°C/min. In the isothermal crystallization experiments for Avrami equation analysis, the sample was first melted on a Linkam HFS901 hot stage at 190°C for 1 min, and then rapidly transferred into DSC equilibrated for the prefixed T_c to allow crystallization. The isothermal crystallization exotherm and the temporal development of crystallization exotherm were recorded; these data were later analyzed according to the usual procedure of evaluating the relative degree of crystallinity $X(t)$:

$$X(t) = \frac{\int_0^t \left(\frac{dH}{dt}\right) dt}{\int_0^\infty \left(\frac{dH}{dt}\right) dt} \quad (1)$$

where the numerator represents the area of isotherms accumulated as of time t and the denominator is the total exotherm area.

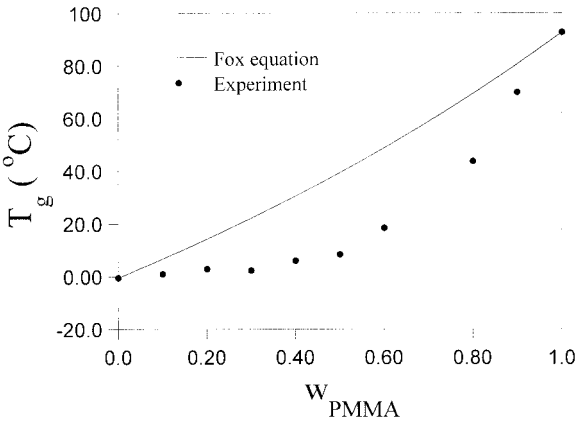

Figure 1 T_g–composition dependency of P(HB-*co*-HV)/PMMA blends.

RESULTS AND DISCUSSION

Miscibility

In general, the miscibility of polymer blends can be determined by thermal characterization. The blends are a miscible system on which a single glass intermediate between those of the two blended polymers is measured. Figure 1 shows the dependency of T_g on PMMA composition (w_{PMMA}). The T_g values of neat P(HB-*co*-HV) and PMMA were −1.2 and 90.5°C, respectively. A single T_g was observed in blends whose value increased with increasing w_{PMMA}. This means that the P(HB-*co*-HV)/PMMA blends were miscible in the melt state. The T_g–composition relation can be expressed well by the theoretical Fox equation[21]

$$\frac{1}{T_{g,\text{blend}}} = \frac{w_{\text{P(HB-}co\text{-HV)}}}{T_{g,\text{P(HB-}co\text{-HV)}}} + \frac{w_{\text{PMMA}}}{T_{g,\text{PMMA}}} \quad (2)$$

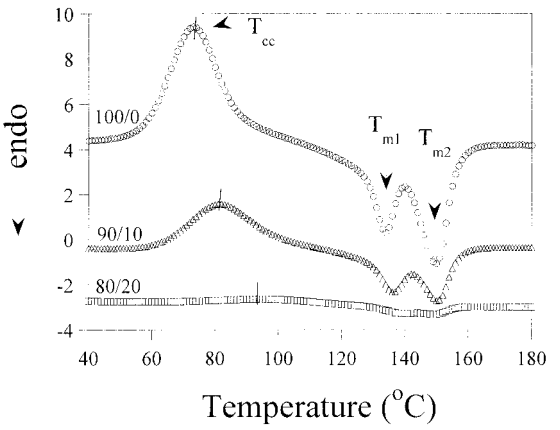

Figure 2 DSC heating scans showing the cold crystallization (T_{cc}) followed by two melting points (T_{m1} and T_{m2}).

where $T_{g,\text{blend}}$, $T_{g,\text{P(HB-}co\text{-HV)}}$, and $T_{g,\text{PMMA}}$ are the T_g values of blend, P(HB-*co*-HV), and PMMA, respectively; and $w_{\text{P(HB-}co\text{-HV)}}$ and w_{PMMA} are the weight fraction of P(HB-*co*-HV) and PMMA, respectively. It may be noticed that the measured T_g was lower than the calculated T_g from the Fox equation, meaning that there was no strong interaction between the P(HB-*co*-HV) and PMMA components. However, it is interesting that the blends of PHB/PMMA,[19,20] prepared by solution casting, formed a glass amorphous single phase with compositions only up to 20 wt % of PHB; at concentrations of PHB higher than 20 wt %, the blends were formed by neat PHB coexisting with a constant composition of 20/80 PHB/PMMA blend. However, the P(HB-*co*-HV)/PMMA blends were completely miscible over the whole composition range.

In addition to the T_g method, the cold crystallization temperature (T_{cc}) and melting point (T_m) in the same heating scan of quenched sample on DSC (at second heating run) can be used together to identify the miscibility of the blends. It is known that T_{cc} must occur at a temperature above the T_g where the crystallizable polymer chains possess enough segmental mobility to crystallize. This indicates that the lower T_g with larger molecular mobility should be accompanied by the lower T_{cc}; inversely, the higher T_g must have a higher T_{cc}. Figure 2 shows DSC thermograms showing T_{cc} and T_m values of each blend composition at a heating rate of 20°C/min. It can be observed that not only did the exotherm decrease but also the T_{cc} shifted toward higher temperature. For the 80/20 composition, the dependency was scarcely noticeable, indicating that the crystallization process occurred from a single homogeneous phase, and the T_g of the blends increased with increasing PMMA attributed to PMMA with higher T_g. This result provides further evidence that the P(HB-*co*-HV)/PMMA blends were miscible in the melt. On the other hand, multiple melting points (T_{m1} and T_{m2}) were also observed in Figure 2. Such multiple melting behavior may be associated with the occurrence of melting, recrystallization, and remelting in the melting region. The T_{m1} is the melting behavior of the original crystals as formed at T_{cc}, whereas the T_{m2} represents the following melt–recrystallization crystals.

Spherulitic morphology

The spherulitic morphology of crystalline polymers can be readily observed by POM. Figure 3 shows the spherulitic structures of P(HB-*co*-HV)/PMMA blends crystallized at T_c = 70°C. No apparent evidence of liquid–liquid phase separation was observed up to impingement of the spherulitic structures, indicating the intraspherulitic segregation of PMMA. Neat P(HB-*co*-HV) exhibited a banded Maltese cross spherulitic structure as neat PHB.[5,16] The banded texture gradually vanished and became faint because of the presence of PMMA disturbing the birefringence of P(HB-*co*-HV) crystals. In addition, the nucleation density was not affected by the addition of PMMA from the observation of spherulitic number.

Equilibrium melting point depression

The miscibility of polymer blends with one crystalline polymer can be determined by melting point depression. Thermodynamic considerations predicted that the chemical potential of a polymer would be decreased by the addition of a miscible dilutent. If one polymer is crystallizable, its decrease in chemical potential will result in a decreased equilibrium melting point (T_m°). The Hoffman–Weeks equation[22] was used to derive T_m° from the relation between the observed melting point (T_m) and the isothermal crystallization temperature (T_c). The Hoffman–Weeks equation[22] is given by

$$T_m = \frac{T_c}{\gamma} + \left(1 - \frac{1}{\gamma}\right) T_m^\circ \qquad (3)$$

where γ is the the ratio of the initial to final lamellar thickness. T_m° was obtained by the extrapolation to the plot of T_m versus T_c, where $T_m = T_c$. In the present study, T_m was conducted on DSC with a heating rate of 20°C/min after the sample crystallized at T_c for 1 h. The DSC scanning thermograms of all isothermally crystallized samples exhibited two melting points (i.e. T_{m1} and T_{m2}), as previously stated in Figure 2: the lower melting point (T_{m1}) was the melting point of the original crystals as formed at the desired T_c, and the other higher melting point (T_{m2}) was distinguished by the melt–recrystallization behavior thus caused. Such a consequence was anticipated because of the tendency of T_{m1} on T_c to have the best-fit linear relation, as shown in Figure 4. In other words, the measured

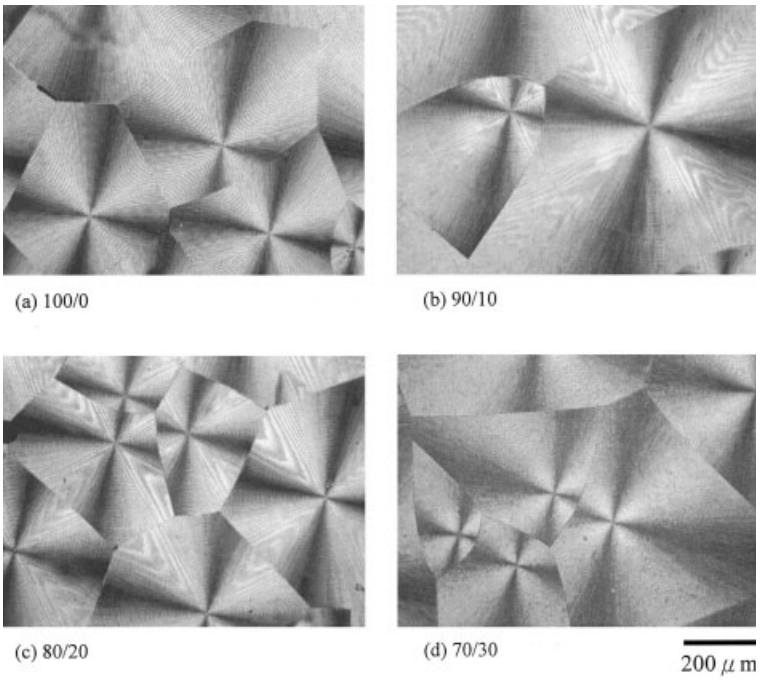

Figure 3 Spherulitic morphologies of P(HB-*co*-HV)/PMMA blends under POM crystallized at T_c = 70°C: (a) 100/0, (b) 90/10, (c) 80/20, (d) 70/30.

T_{m1} linearly increased with increasing T_c. Table I lists the values of T_m° obtained from Figure 4. It is clearly seen that T_m° decreased with increasing PMMA, meaning that the P(HB-*co*-HV)/PMMA blends were a miscible system in the melt state.

Spherulitic growth

The spherulitic radial growth rates (G) of neat P(HB-*co*-HV) and P(HB-*co*-HV)/PMMA blends were determined by measuring the spherulitic radii R at various time periods during isothermal crystallization. For each composition studied, R was observed to increase linearly with time up to the point of impingement, indicating a constant growth rate throughout the crystallization process. The linearity of R implies that the PMMA component, which is segregated away from the crystal growth front, does not accumulate at the spherulitic growth front, but should be trapped within the interlamellar or interfibrillar regions in the growing spherulites. Figure 5 depicts the variation of spherulitic growth rate G with increasing T_c at each blend composition. It is observed that G decreased significantly with increasing PMMA composition at a given T_c. Such a dramatic reduction in growth rate has been widely observed in blends[23–25] with an amorphous polymer with a higher T_g, which was attributed to the decrease of molecular mobility and the dilution of the crystalline component. The decrease of equilibrium melting point attributed to segmental miscibility may also contribute to the reduction of crystallization kinetics in miscible polymer blends, although this effect is usually less significant for a system with rela-

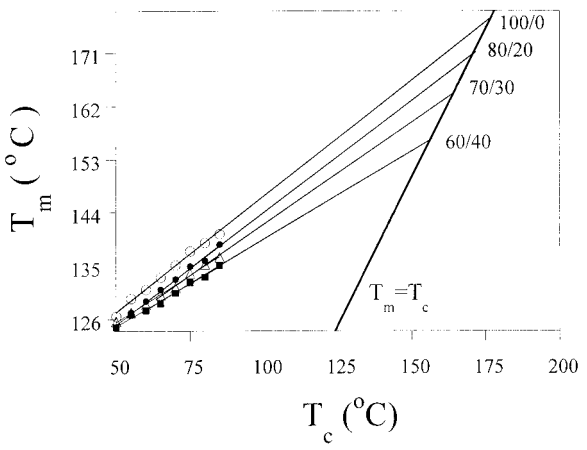

Figure 4 Plot of the Hoffman–Weeks equation for P(HB-*co*-HV)/PMMA blends.

TABLE I
Equilibrium Melting Points (T_m°) of P(HB-*co*-HV)/PMMA Blends

P(HB-*co*-HV)/PMMA	T_m° (°C)
100/0	176.5
90/10	174.5
80/20	171.1
70/30	160.0
60/40	155.3

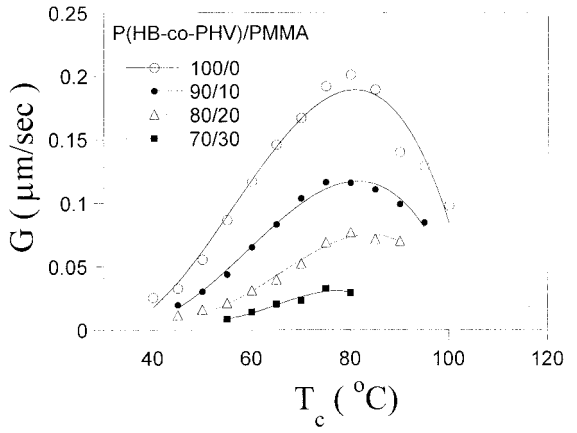

Figure 5 Variation of the spherulitic growth rate as a function of crystallization temperature.

tively weak interactions. Similarly, the same reason may be cited to explain the growth rate depression in the P(HB-*co*-HV)/PMMA system.

On the other hand, the trend of curves in Figure 5 shows the maximum of G in the neighborhood of 80°C at each composition. It is well known that the crystallization window of a crystalline polymer must lie between T_g and T_m°. When the desired T_c values are located near T_g, the crystallization kinetics would be controlled by the chain mobility, such that the rate increases with increasing T_c in this mobility regime. In contrast, if the desired T_c values are located near T_m°, the crystallization rate would be controlled by the thermodynamic driving force of crystallization (the thermodynamically controlled regime). The interplay between these two factors produces a maximum in the crystallization rate at $T_c^{\max}$ between T_g and T_m°. It is observed that the $T_c^{\max}$ values of neat P(HB-*co*-HV) and P(HB-*co*-HV)/PMMA blends were around 80°C.

The relation of the spherulitic radial growth of blends containing crystallizable polymer with composition has been described by the Hoffman–Lauritzen theoretical equation,[26,27] as expressed in eq. (4), which was used to analyze the experimental data of G.

$$G = G_0 \exp[-U^*/R(T_c - T_\infty)] \exp[-K_g/T_c(\Delta T)f] \quad (4)$$

where G_0 is a preexponential factor that is essentially independent of temperature; U^* is the activation energy for transportation of crystallizable segments to the crystallization front; T_∞ is the temperature below which such motions cease; ΔT is the degree of undercooling ($\Delta T = T_m^\circ - T_c$); and f is a correlation factor that accounts for the variation of the heat of fusion on temperature and is written as $f = 2T_c/(T_m^\circ + T_c)$. The nucleation factor K_g is expressed by[26,27]

$$K_g = \frac{nb_0\sigma\sigma_e T_m^\circ}{\Delta H^\circ k} \quad (5)$$

where σ and σ_e are the lateral and end-surface free energies, respectively, of the growing crystal; b_0 is the molecular thickness; k is the Boltzmann constant, and ΔH° is the heat of fusion of crystals. According to Hoffman–Lauritzen theory,[26,27] the value of n depends on the regime of crystallization. At high T_c values (low ΔT) each surface nucleation occurrence results in rapid completion of the growth strip before the next nucleation event. This is distinguished as regime I and $n = 4$. At lower T_c values (medium ΔT), in regime II, multiple surface nuclei form on the substrate and $n = 2$. When crystallization occurs at much lower T_c values, the separation between the multiple nuclei characteristic of regime II reaches its minimum value. This is regime III (high ΔT) and $n = 4$.

It is important to note that the parameters U^* and T_∞ were treated as variables to maximize the quality of the fit to eq. (4). In many cases in the literature these parameters have simply been assigned the values[26] $U^* = 1500$ cal/mol and $T_\infty = T_g - 30$ K, as appropriate to many polymers, or the Williams–Landel–Ferry (WLF) values[28] $U^* = 4120$ cal/mol and $T_\infty = T_g - 51.6$ K. However, the parameter U^* was treated as a variable to achieve a good quality of fit to eq. (4). In the present study, $U^* = 2600$ cal/mol and $C = 51.6$ K, and T_m° values in Table I were applied to achieve a very good fit to the plot of $\ln G + U^*/R(T_c - T_\infty)$ versus $1/(fT_c\Delta T)$, as seen in Figure 6. Table II lists the values of K_g calculated by the slope of the straight line in Figure 6. It is found that all the K_g values were closely approximate to that of neat PHB as previously reported.[16,29] Barham et al.[16] found that neat PHB crystallizes according to regime III for the present undercoolings. Therefore, the resulting K_g values of P(HB-*co*-HV)/PMMA blends as listed in Table II are also assigned to be regime III and thus $n = 4$. In other words, the crystallization process of HB units in the investigated copolymers was unaffected by the existence of HV content and the addition of PMMA.

The value of σ was calculated by the empirical equation[30]

$$\sigma = \alpha(\Delta H^\circ)(a_0 b_0)^{1/2} \quad (6)$$

Here, we assumed that the crystal of HB lattice in P(HB-*co*-HV) studied is the same as that of neat PHB so that these parameters[16] $\Delta H^\circ = 1.85 \times 10^8$ J/m^3, $a_0 = 6.6$ Å, and $b_0 = 5.8$ Å of neat PHB can be adopted. In general, the value of $\alpha = 1$ is widely used in polyethylene[26] and other flexible polymers.[30] Roitman[31] and Marand and Hoffman[32] found that the value of $\alpha = 0.25$ was appropriate for higher melting polymers such as polypivalolactone. Here, eq. (6) with $\alpha = 0.25$ yielded $\sigma = 28.6$ erg/cm^2, which was consistent with reported values in the literature for neat PHB,[16] P(HB-*co*-HV),[33] and blends with PHB.[9,29] Furthermore, the values of σ_e were obtained by eq. (5)

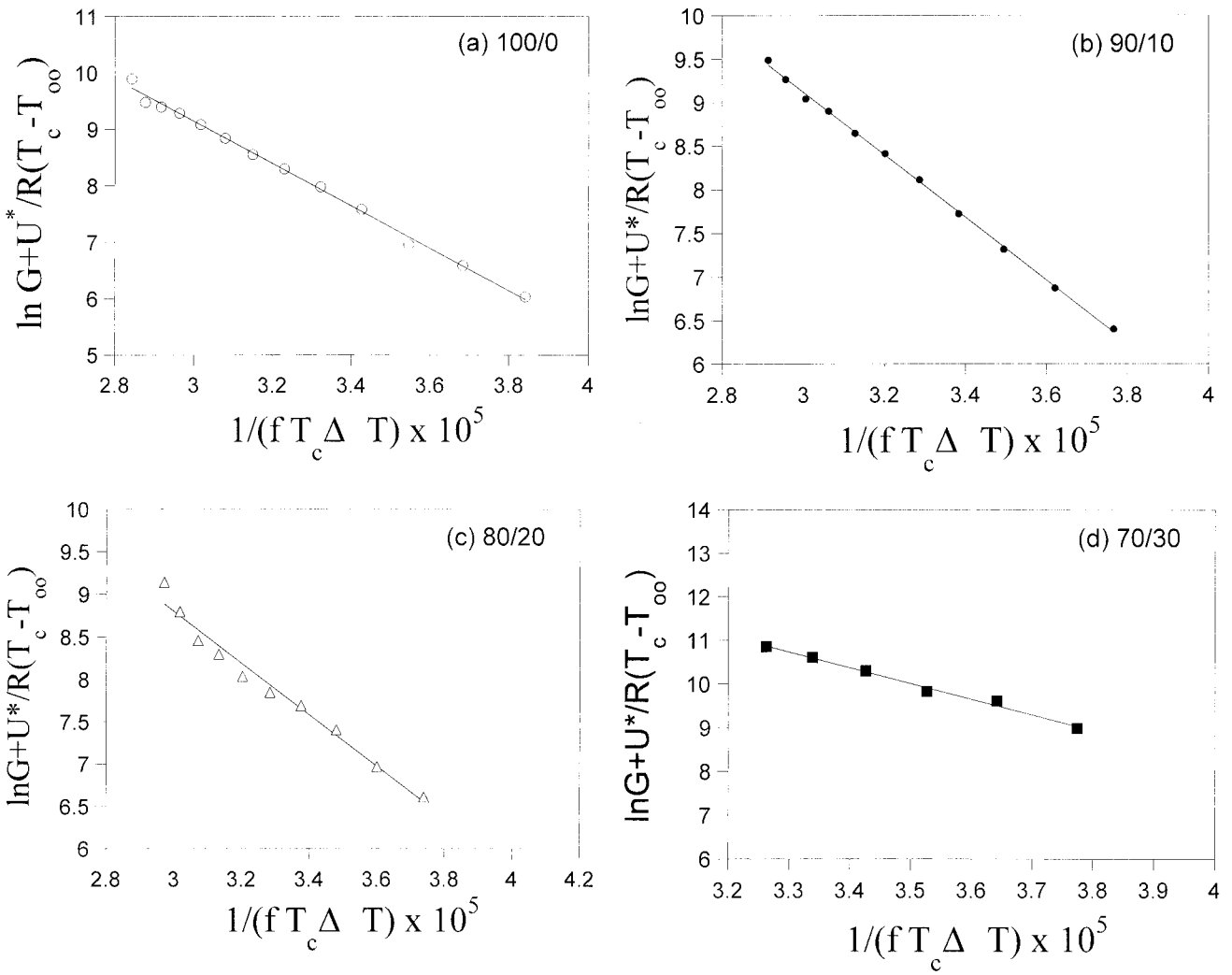

Figure 6 Plots of ln $G + U^*/R(T_c - T_\infty)$ versus $1/(fT_c\Delta T) \times 10^5$ for P(HB-*co*-HV)/PMMA blends: (a) 100/0, (b) 90/10, (c) 80/20, (d) 70/30.

(i.e., K_g), also listed in Table II. The values of σ_e were in agreement with a previously reported value of 38 $\pm$ 6 erg/cm^2 determined by measurements of lamellar thickness for neat PHB.[16] q is given by[26]

$$q = 2a_0b_0\sigma_e \quad (7)$$

The variable q was previously reported to be the one parameter most closely correlated with the molecular structure and the magnitude of q is roughly proportional to chain stiffness.[26] It has been found that polyethylene and poly(ϵ-caprolactone) with moderately stiff chains without a side group have a value of $q \sim 5$ kcal/mol[34,35] and polystyrene with bulky side groups has a value of $q \sim 7$ kcal/mol.[36] Consequently, the value of q = 3.5 kcal/mol of neat P(HB-*co*-HV) fit into the category of moderately stiff chains. Pearce and Marchessault[37] found that neat PHV had a value of 2.2 kcal/mol of q with α = 0.25 and it was difficult to

TABLE II
Values of K_g, σ_e, and q of P(HB-*co*-HV)/PMMA Blends

P(HB-*co*-HV)/PMMA	K_g	Regime	Correlation coefficient	σ_e (erg/cm^2)	q (kcal/mol)
100/0	3.7511×10^5	III	0.9980	32.2	3.5
90/10	3.5967×10^5	III	0.9995	31.0	3.4
80/20	3.0382×10^5	III	0.9886	26.4	2.9
70/30	3.5969×10^5	III	0.9952	31.8	3.8

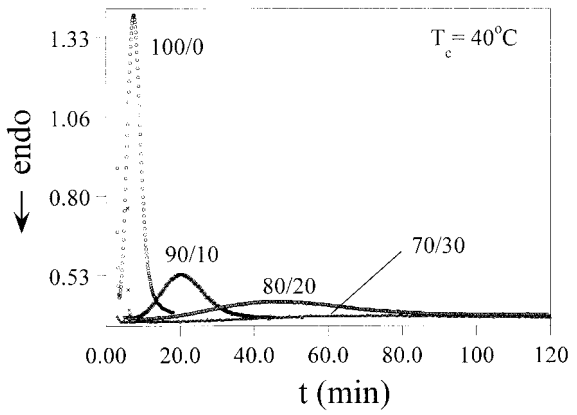

Figure 7 Crystallization exotherm of P(HB-*co*-HV)/PMMA blends at T_c = 40°C.

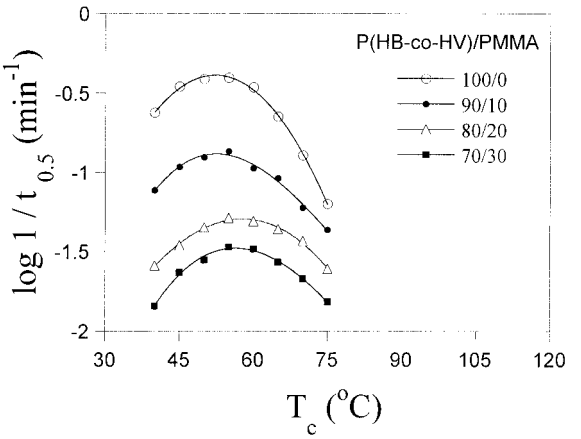

Figure 9 Variation of log $1/t_{0.5}$ as a function of crystallization temperature.

justify a value much lower than this for neat PHV, which has a longer side chain than that of neat P(HB-*co*-HV).

Overall crystallization kinetics

It is well known that the overall crystallization rate is determined by both the nucleation and growth rates. Figure 7 displays the crystallization exotherm dependency on crystallization time at T_c = 40°C. It is observed that the exothermic peak shifted to a greater amount of time and the height in the peak decreased with increasing PMMA. For the 70/30 composition, the exothermic peak was not observed because of extremely slow crystallization so that the exotherm could not be observed. Figure 8 shows the temporal development of $X(t)$ of each blend composition at T_c = 40°C. It can be seen that the crystallization isotherms displayed the characteristic sigmoidal shape. Furthermore, the initial slope of the isotherms decreased with increasing PMMA, indicating a progressively slower crystallization rate. This means that the presence of PMMA would strongly retard the overall crystallization kinetics of P(HB-*co*-HV). The half-time of crystallization $t_{0.5}$, defined as the time required to attain half of the final crystallinity, was evaluated from these curves. The overall crystallization rate can be represented by $1/t_{0.5}$. Figure 9 displays the dependency of log $1/t_{0.5}$ on crystallization temperature. It is clearly observed that the overall crystallization rate ($1/t_{0.5}$) decreased with increasing PMMA at a given T_c, which was primarily attributed to the reduction of molecular mobility arising from the increase of T_g upon blending with PMMA. In addition, the curve of log $1/t_{0.5}$ also exhibited a maximum ($1/t_{0.5}^{max}$), which was also attributed to the coupling of the chain mobility and the thermodynamic driving force of controlled crystallization.

To obtain further details concerning the overall crystallization kinetics of neat P(HB-*co*-HV) and P(HB-*co*-HV)/PMMA blends, the kinetics of the overall crystallization of each sample was further analyzed on the basis of the Avrami equation[38–40]

$$\ln\{-\ln[1 - X(t)]\} = \ln k + n_{av}\ln t \qquad (8)$$

where k is the overall crystallization rate constant containing contributions from both nucleation and growth rate, and n_{av} is the Avrami exponent that depends on the nucleation and growth mechanism of the crystals. The plot of $\ln\{-\ln[1 - X(t)]\}$ versus $\ln t$ produces a linear line with intercept and slope given by k and n_{av}, respectively. Figure 10 displays the Avrami plot of each blend composition at T_c = 40°C. It can be seen that the experimental data closely agree with the Avrami equation at low conversion. Plots at high conversion deviate from the equation as the result of secondary crystallization. Similar to the values reported for blends,[40–42] all the values of n_{av} obtained were between 2 and 3. Such values of n_{av} were sug-

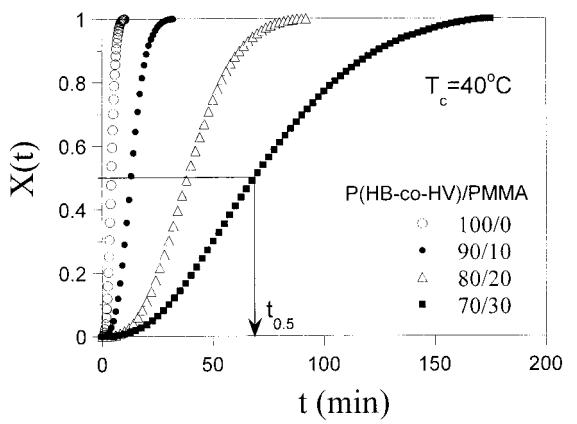

Figure 8 Temporal development of $X(t)$ of P(HB-*co*-HV)/PMMA blends at T_c = 40°C.

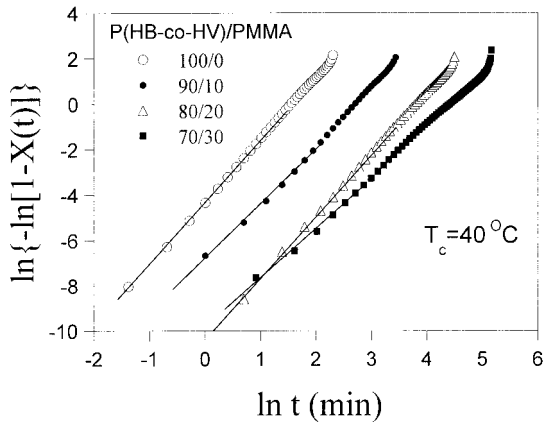

Figure 10 Plot of the Avrami equation for P(HB-*co*-HV)/PMMA blends at T_c = 40°C.

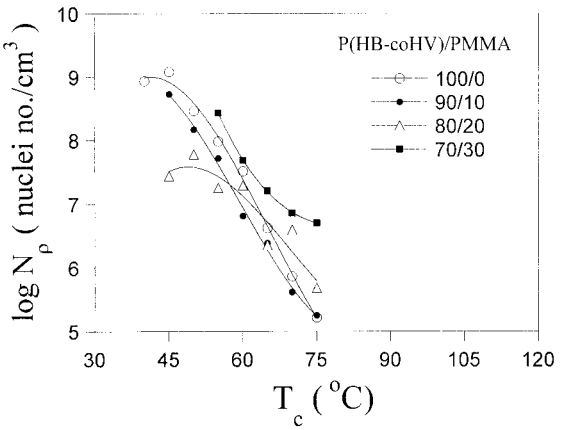

Figure 12 Variation of log N_ρ as a function of crystallization temperature.

gested to be attributable to the existence of mixed growth, surface nucleation, and two-step crystallization. However, although all n_{av} values of the studied samples were lower than 3, these results may roughly confirm a three-dimensional (spherulitic) growth process initiated by heterogeneous nucleation, which was consistent with the observed spherulitic morphology by POM in Figure 3.

The rate constant defined eq. (8) has a unit of $\text{min}^{-n_{av}}$. In this study, we modified the rate constant as $k_n = k^{1/n_{av}}$ to unify the unit of the rate constant as min^{-1}. Figure 11 depicts the dependency of log k_n on crystallization temperature. The trend of k_n was similar to that of $1/t_{0.5}$ as in Figure 9. It should be noted that k_n contains a contribution from both nucleation and growth rates. Because Figure 3 suggests that the nucleation density (rate) was not enhanced in the blends, the depression of k_n with the addition of PMMA implies that the composition effect on the overall crystallization kinetics was dominated by the crystal growth rate. On the other hand, all the temperatures corresponding to k_n^{max} were located in the region of the lower temperature of G^{max} in Figure 5. In other words, the temperatures relating to k_n^{max} (or $1/t_{0.5}^{max}$) were different from those of G^{max} in Figure 5. In the investigation of poly(ether ether ketone) (PEEK)/polyether imide (PEI) blends, Chen et al.[44] suggested that the variation of nucleation rate with the degree of undercooling was more susceptible than the growth rate, given that the primary nucleation rate varies with $\exp(-1/\Delta T^2)$, whereas the growth rate varies with $\exp(-1/\Delta T)$. In other words, the nucleation rate was decreased by a greater extent upon the decrease of ΔT. In this study, we found that T_m° decreased with increasing PMMA, as previously stated in Figure 4, meaning the decrease of T_m° lowered the value of ΔT, which resulted in the greater degree of depression of k_n. This suggestion indicates that the discrepancy in temperatures relating to k_n^{max} and G^{max} may be mainly attributed to the larger depression of nucleation rate than that of G.

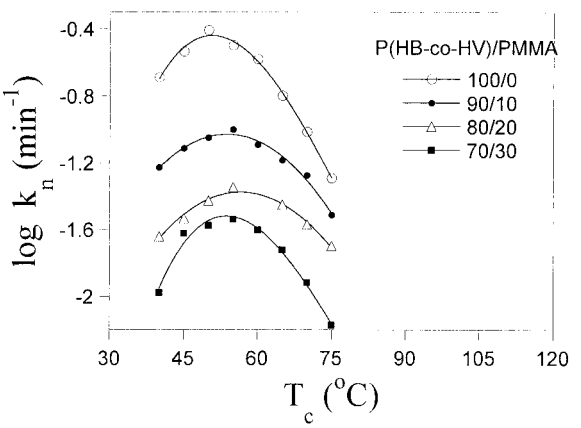

Figure 11 Variation of log k_n as a function of crystallization temperature.

According to three-dimensional spherulitic growth, k is defined as

$$k = 4\pi N_\rho (G)^3/3 \tag{9}$$

where N_ρ is the nucleation density corresponding to the number of nuclei per cm^3. From eq. (9) the values of N_ρ were calculated. Figure 12 depicts the dependency of log N_ρ on crystallization temperature. It can be seen that log N_ρ was independent of blend composition at certain T_c. In other words, the addition of PMMA did not affect the nucleation density of P(HB-*co*-HV). This result confirms the previous observation of spherulitic morphology in Figure 3 and further supports the previous suggestion that the overall crystallization rate was mainly governed by the growth rate. In addition, it is obvious that log N_ρ decreased dramatically with increasing T_c because of the decrease in the degree of undercooling ($\Delta T = T_m^\circ - T_c$).

CONCLUSIONS

The miscibility and crystallization kinetics of P(HB-*co*-HV)/PMMA blends were investigated by DSC and POM. The single glass-transition temperatures of the blends within the whole composition range suggest that P(HB-*co*-HV)/PMMA blends were totally miscible in the melt. The equilibrium melting point of P(HB-*co*-HV), in the P(HB-*co*-HV)/PMMA blends from the Hoffman–Weeks equation analysis, decreased with increasing of PMMA. The spherulitic morphologies of P(HB-*co*-HV)/PMMA blends indicated that PMMA was predominantly segregated into P(HB-*co*-HV) interlamellar and/or interfibrillar regions after P(HB-*co*-HV) crystallization. The results of a crystallization kinetics study revealed that the overall crystallization rate and crystal growth kinetics decreased upon the addition of PMMA. The kinetics retardation was primarily attributed to the reduction of P(HB-*co*-HV) chain mobility and dilution of P(HB-*co*-HV) upon mixing with PMMA. The kinetics of spherulitic crystallization of neat P(HB-*co*-HV) and P(HB-*co*-HV)/PMMA blends were analyzed by the secondary nucleation theory. Consequently, the crystallization of neat PHB-*co*-HV and P(HB-*co*-HV)/PMMA blends were assigned to $n = 4$, regime III growth process. For the present blend compositions and T_c values studied, the overall crystallization kinetics was dominated by the growth rate. The underlying nucleation mechanism and growth geometry of P(HB-*co*-HV) crystals were not affected by blending, as confirmed from the results of Avrami analysis.

This work is supported by the National Science Council, Republic of China, under Grant NSC 91-2216-E-233-001.

References

1. Paglia, E. D.; Beltrame, P. L.; Canetti, M.; Seves, A.; Marcandalli, B.; Martuscelli, E. Polymer 1993, 34, 996.
2. Sadocco, P.; Canetti, M.; Seves, A.; Martuscelli, E. Polymer 1993, 34, 3368.
3. Greco, P.; Martuscelli, E. Polymer 1989, 30, 1475.
4. An, Y.; Dong, L.; Xing, P.; Mo, Z.; Zhuang, Y.; Feng, Z. Eur Polym Mater 1997, 33, 1449.
5. Chiu, H. J.; Chen H. L.; Lin, T. L.; Lin, J. S. Macromolecules 1999, 32, 4969.
6. Peace, R.; Brown, G. R.; Marchessault, R. H. Polymer 1994, 35, 3984.
7. Abe, H.; Doi, Y.; Satkowski, M. M.; Noda, I. Macromolecules 1994, 27, 50.
8. Iriondo, P.; Iruin, J. J.; Fernandez-Berrodi, M. J. Polymer 1995, 36, 3235.
9. Xing, P.; Dong, L.; An, Y.; Feng, Z.; Avella, M.; Martuscelli, E. Macromolecules 1997, 30, 2726.
10. Chitrangad, B.; Middleman, S. Macromolecules 1981, 14, 352.
11. Liu, A. S.; Liar, W. B.; Chiu, W. Y. Macromolecules 1998, 31, 6593.
12. Martuscelli, E.; Silverstre, C.; Gismondi, C. Makromol Chem 1985, 186, 16.
13. Alfonso, G. C.; Russell, T. P. Macromolecules 1986, 19, 1143.
14. Greveceur, G.; Groeninckx, G. Macromolecules 1991, 24, 1190.
15. Cheung, Y. W.; Stein, R. S. Macromolecules 1994, 27, 2512.
16. Barham, P. J.; Keller, A.; Otun, E. L.; Holmes, P. A. J Mater Sci 1984, 19, 2781.
17. Griffin, G. J. L. Chemistry and Technology of Biodegradable Polymers; p. 48.
18. Erhoogt, H.; Ramsay, B. A.; Favis, B. D. Polymer 1994, 35, 5155.
19. Lotti, N.; Pizzoli, M.; Ceccorulli, G.; Scandola, M. Polymer 1993, 34, 35.
20. Sicilano, A.; Seves, A.; Marco, T. D.; Cimmino, S.; Martuscelli, E. Macromolecules 1995, 28, 8065.
21. Fox, T. G. Bull Am Phys Soc 1956, 2, 1123.
22. Hoffman, J. D.; Weeks, J. J. J Res Natl Bur Stand (US) 1962, 66A, B.
23. Flory, P. J. J Chem Phys 1949, 17, 223.
24. Mandelkern, L. J Appl Phys 1955, 26, 443.
25. Boon, J.; Azcue, J. M. J Polym Sci Polym Phys Ed 1968, 6, 885.
26. Hoffman, J. D.; Davis, G. T.; Lauritzen, J. I., Jr. In: Treatise on Solid State Chemistry, Vol. 3; Hannay, N. B., Ed.; Plenum Press: New York, 1976.
27. Hoffman, J. D. Polymer 1983, 24, 3.
28. Williams, M. L.; Landel, R. F.; Ferry, J. D. J Am Chem Soc 1955, 77, 3701.
29. Xing, P.; Ai, X.; Dong, L.; Feng, Z. Macromolecules 1998, 31, 6898.
30. Lauritzen, J. I., Jr.; Hoffman, J. D. J Appl Phys 1973, 44, 4340.
31. Roitman, D. B.; Marand, H.; Miller, R. L.; Hoffman, J. D. J Phys Chem 1989, 93, 6919.
32. Marand, H. J.; Hoffman, D. Macromolecules 1990, 23, 3682.
33. You, J. W.; Chiu, H. J.; Shu, W. J.; Don, T. M. J Polym Res 2003, 10, 47.
34. Hoffman, J. D.; Miller, R. L. Macromolecules 1988, 21, 3038.
35. Philips, P. J.; Rensch, G. H.; Taylor, K. D. J Polym Sci Polym Phys Ed 1987, 25, 27.
36. Hoffman, J. D.; Miller, R. L.; Marand, H.; Roitaman, D. B. Macromolecules 1992, 25, 2221.
37. Pearce, R. P.; Marchessault, R. H. Macromolecules 1994, 27, 3869.
38. Avrami, M. J Chem Phys 1939, 7, 1130.
39. Avrami, M. J Chem Phys 1940, 8, 212.
40. Avrami, M. J Chem Phys 1941, 9, 177.
41. Hay, J. N.; Sharma, L. Polymer 2000, 41, 5799.
42. Lisowski, M. S.; Liu, Q.; Cho, J.; Runt, J. Macromolecules 2000, 34, 4842.
43. Grenier, D.; Prud'hamme, R. J Polym Sci Polym Phys Ed 1980, 18, 1655.
44. Chen, H.-L.; Porter, R. S. J Polym Res 1999, 6, 21.